Combustion and Flame 164 (2016) 319–328

Contents lists available at ScienceDirect

Combustion and Flame

journal homepage: www.elsevier.com/locate/combustflame

Interactions of flame propagation, auto-ignition and pressure wave during knocking combustion

Jiaying Pan [a], Gequn Shu [a], Peng Zhao [b], Haiqiao Wei [a,*], Zheng Chen [c]

[a] State Key Laboratory of Engines, Tianjin University, Tianjin 300072, China
[b] Department of Mechanical Engineering, Oakland University, Rochester, MI 48309, USA
[c] SKLTCS, Department of Mechanics and Engineering Science, Peking University, Beijing 100871, China

ARTICLE INFO

Article history:
Received 14 July 2015
Revised 26 November 2015
Accepted 27 November 2015
Available online 29 December 2015

Keywords:
Knocking combustion
Flame propagation
Auto-ignition
Pressure wave
Detonation

ABSTRACT

Using one-dimensional numerical simulation, the interactions of flame propagation, auto-ignition and pressure wave during various knocking combustion scenarios are systematically investigated, for stoichiometric H_2–air mixture fueled in a closed constant volume reactor. Different types of auto-ignition and pressure mutation are identified with various initial temperatures. It is found that as initial temperature increases, there is a transition for the auto-ignition (AI) position from the near-wall region to the region ahead of SI flame front, resulting in distinct pressure mutation and knocking intensity. Further analysis on sequential knocking combustion demonstrates that knocking intensity not only corresponds to the initial auto-ignition events induced by thermal inhomogeneity, but also to the subsequent interactions of flame front propagation, as well as AI spots initiation and pressure wave generation. Consequently, more intense pressure mutation could result from the developing detonations. Finally, the mechanism of AI occurrence and AI development is identified, which demonstrates the essential role of pressure wave disturbance in the formation of thermal inhomogeneity and detonations.

1. Introduction

Recently engine downsizing with supercharging technology has become increasingly attractive in spark-ignited (SI) engines because of its higher thermal efficiency and lower emissions [1]. However, the required increments in Brake Mean Effective Pressure (BMEP) induce severe thermodynamic conditions, which promote the possibilities of abnormal combustion phenomena prior to or during engine combustion, such as knock or super-knock [2–3], both of which are supposed to be induced by auto-ignition (AI) events during premixed combustion. Auto-ignition originates from a single or multiple hot (or cold) spots by which a combustible mixture reacts in a self-accelerating manner, and eventually becomes explosive, leading to fully fledged combustion followed by intense pressure mutations [4]. Although extensive numerical and experimental work has been done, there is still lack of understanding on the generation of the strong pressure wave during knocking combustion and the process of detonation development in such limited space during engine combustion [5].

Recent study on knocking combustion can be traced to the flame propagation and end-gas auto-ignition with thermal and concentration stratifications in the charge. A pioneering work by Zel'dovich [6] pointed out that there are different combustion modes for a flame front propagating in the charge with non-uniform reactivity. Later, Bradley, Gu and Kalghatgi [7–9] developed a theoretical relation based on a group of dimensionless parameters (ξ, ε), representing the normalized temperature gradient and the ratio of acoustic time to excitation time respectively, to describe the limits of developing detonation mode based on H_2–CO–air and H_2–air mixtures. Griffiths [10] and Dai et al. [11] studied the negative temperature coefficient (NTC) behavior of end-gas auto-ignition, suggesting the essential role of AI heat release and pressure wave in subsequent evolution of combustion behaviors. However, due to the artificially introduced temperature gradients and lack of modeling SI flame propagation, the influence of flame front propagation on end-gas auto-ignition and their interactions have been neglected in most of these investigations.

To study the interactions of flame front propagation and end-gas auto-ignition, Pitz and Westbrook [12] firstly examined the transient behavior of a laminar reaction front propagating into the auto-igniting mixture near the wall region, and found that high heat release rate during end-gas auto-ignition could generate strong pressure waves. Further, Martz et al. [13–14] performed one-dimensional

* Corresponding author. Fax: +862227402609.
E-mail address: whq@tju.edu.cn (H. Wei).

http://dx.doi.org/10.1016/j.combustflame.2015.11.030
0010-2180/

(1D) steady and unsteady numerical simulations for a laminar reaction front propagating into an auto-igniting mixture, and found that the reaction progress of end auto-igniting mixture significantly influences the combustion regime transitions of propagating flame fronts. Unfortunately, the physics related to transient pressure waves was not accounted for in their models. A numerical work by Ju et al. [15] suggested that there are at least six different combustion regimes at near NTC temperatures during the dynamic interactions between flame front propagation and end-gas auto-ignition. However, the mechanism of strong pressure wave generation and the subsequent influence on flame front dynamics was not addressed.

The interactions of flame front propagation, end-gas auto-ignition and pressure wave are very complicated but extremely crucial during knocking combustion, which affect the characteristics of local pressure mutation, combustion regime transitions and knocking intensity. Robert et al. [16] used 15 LES cycles of a high load/low speed SI engine operations to visualize the knocking and super-knocking combustion, and found that the coupling of pressure wave, AI spots and AI heat release may contribute to a deflagration to detonation transition (DDT). However, the empirical models utilized in their three dimensional (3D) simulation prevent a deeper physical understanding on the detailed processes for such interactions. A 1D direct numerical simulation was performed by Terashima et al. [17] on the pressure wave induced by the end-gas auto-ignition. However, an essential process of transient pressure mutation resulting from the flame front-wave interaction was not demonstrated. Additionally, the actual physical process for flame front propagation, end-gas auto-ignition and pressure (or shock) wave during knocking combustion spans up to 12 orders of magnitude in terms of the time scale [18], it is reasonable to utilize an advanced algorithm like adaptive mesh refinement to improve numerical fidelity and computational efficiency.

This study aims to demonstrate the underlying mechanism during the interactions of flame propagation, auto-ignition and pressure wave during knocking combustion, with special emphasis on auto-ignition occurrence and pressure mutation generation. The paper was organized as follows. Flame front initiation, propagation and AI generation in constant volume reactor filled with homogeneous stoichiometric H_2–air mixture were firstly studied under different initial temperatures to visualize various scenarios of engine knocking combustion. Then the sequential interactions of flame front propagation, auto-ignition and pressure wave were discussed, followed by analysis based on the evolution of thermodynamic conditions, different velocity scales associated with each phenomenon, and the temperature inhomogeneity. Finally, to demonstrate the essential role of pressure wave in the formation of thermal inhomogeneity and detonation wave, the effects from chamber lengths and thermodynamic states of local mixture in flame preheat zone were analyzed.

2. Methodology and models

2.1. Governing equations

In order to resolve the multi-physical problem involving flame propagation, auto-ignition and pressure wave, a time-accurate and space-adaptive numerical solver for Adaptive Simulation of Unsteady Reactive (A-SURF) is used to perform high-fidelity numerical simulations. The unsteady Navier–Stokes equations and the energy and species conservation equations for a multi-components reactive mixture in a 1D rectangular coordinate are solved in the A-SURF [19]:

$$\frac{\partial U}{\partial t}+\frac{\partial F(U)}{\partial x}=\frac{\partial F_v(U)}{\partial x}+S_R \tag{1}$$

where the vectors U, $F(U)$, $F_v(U)$ and S_R are defined as:

$$U=\begin{pmatrix} pY_1\\ pY_2\\ \cdot\\ \cdot\\ \cdot\\ pY_N\\ pu\\ E\end{pmatrix},\ F(U)=\begin{pmatrix} puY_1\\ puY_2\\ \cdot\\ \cdot\\ \cdot\\ puY_N\\ pu^2+P\\ (E+P)u\end{pmatrix},$$

$$F_v(U)=\begin{pmatrix} -puY_1V'_1\\ -puY_2V'_2\\ \cdot\\ \cdot\\ \cdot\\ -pY_nV'_n\\ \tau\\ q\end{pmatrix},\ S=\begin{pmatrix}\omega\\ \omega\\ \cdot\\ \cdot\\ \cdot\\ \omega_n\\ 0\\ 0\end{pmatrix} \tag{2}$$

Here ρ is the density, u the flow velocity and E the total energy per unit volume, and Y_K, V'_K and ω_K are the mass fraction, diffusion velocity and production rate of specie K, respectively. The production rate of species K, ω_K, due to chemical reaction is specified via collection of elementary reactions using a CHEMKIN compatible database [20]. The mixture-averaged method is employed to calculate diffusion velocity and the Soret diffusion effect of H and H_2 is considered. In the momentum equation, P is hydrostatic pressure and τ is viscous tress tensor represented by $\tau=\mu(2S)-\frac{2}{3}\mu(\nabla\cdot u)\delta$, where μ is the viscosity of the mixture and S the symmetric strain rate tensor. In the energy conservation equation, the total energy, E, is defined through

$$E=-P+\frac{pu^2}{2}+ph,\quad h=\sum\nolimits_{K=1}^{K=n}(Y_Kh_K),$$
$$h_K=h_{(K,0)}+\int_{T_0}^{T}C_{P,K}(T)dT \tag{3}$$

where T is the temperature, h_K the enthalpy of species K, $h_{K,0}$ the species enthalpy of formation at the reference temperature T_0 and $C_{P,K}$ the specific heat of species K at constant pressure. The heat flux q is defined as

$$q=-\lambda\nabla T+\rho\sum\nolimits_{K=1}^{K=n}\left(h_kY_kV'_K\right) \tag{4}$$

where λ is thermal conductivity of mixture.

A-SURF has been successfully used in the research of auto-ignition, flame propagation, shock wave propagation and detonation combustion, and the more details on numerical schemes and code validation can be found in the paper [11,19,21–22].

2.2. Numerical methodology

During the simulations, the second-order accurate, Strang splitting fractional-step procedure is adopted in order to separate the time evolution of stiff reaction term from that of the convection and diffusion terms. In the first fractional step, the non-reactive flow is resolved and Runge–Kutta, MUSCL-Hancock and central difference schemes, all with second-order accuracy, are employed to calculate temporal integration, convective and diffusion flux, respectively. The second fractional step is to solve the chemistry term using the VODE solver. Meanwhile, a multi-level algorithm with adaptive mesh refinement has been applied based on the first-order and second-order gradient of temperature, velocity and major species distributions to guarantee adequate numerical resolutions for the propagating flame front, end-gas auto-ignition and pressure waves [23]. Moreover, a finest mesh of 1 μm and the corresponding time step is 8×10^{-11} s is utilized in the current work.

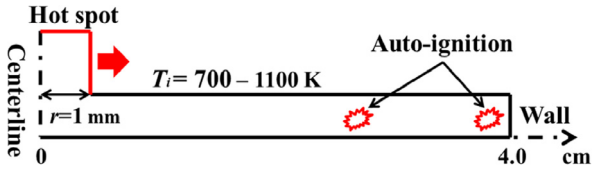

Fig. 1. Schematic of the constant volume reactor.

2.3. Physical model

A 1D planar constant volume reactor is modeled to represent the combustion chamber for a SI engine piston located at the top dead center (TDC). It should be noted that this work is mainly to understand laminar combustion regime, so turbulence is not considered. Symmetric boundary condition is used at the centerline of the reactor and the length of the computation domain is reduced to L =4.0 cm. Adiabatic and reflective boundary conditions are utilized for wall boundaries. Initially, a 1.0 mm-thick artificial hot spot with average temperature of 1450 K is created at the left boundary, which is surrounded by quiescent homogeneous H_2–air mixture at initial temperature of T_i =700–1100 K, fixed initial pressure of P_0 =4.5 atm and equivalence ratio of ϕ =1.0. Then a flame front induced will propagate towards the wall side. AI spots may take place in the unburned region near the flame front or by the wall side, depending on the local temperature and pressure history. It should be noted that in addition to the initial temperature of the mixture, the initial temperature of a hot spot also affects combustion process, especially for the initiation of the flame front, which is nevertheless beyond the scope of the current research. The schematic of the constant volume reactor is shown in Fig. 1. The chemical kinetic mechanism adopted here is an updated comprehensive H_2 kinetic model for high-pressure combustion [24], which has been tested against a wide range of combustion targets including recent high-pressure flame speeds data, with updated rate constants.

3. Results and discussion

3.1. Propagation of deflagration and auto-ignition initiated detonation

Figure 2 shows the profile of a flame front propagating in the reactor at different initial temperatures of T_i =700, 1000 and 1050 K. Here, the flame front is defined as the position with local peak heat release rate. It is observed that for the T_i =700 K case, a flame front gradually propagates towards the right wall with a mean deflagration flame

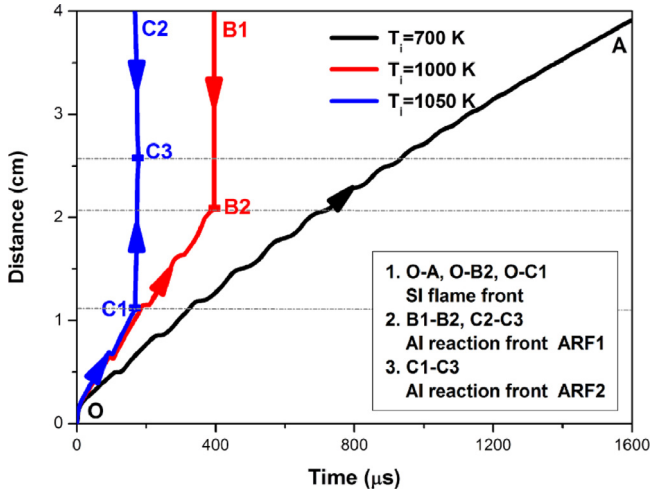

Fig. 2. Profile of flame front propagation at different initial temperatures.

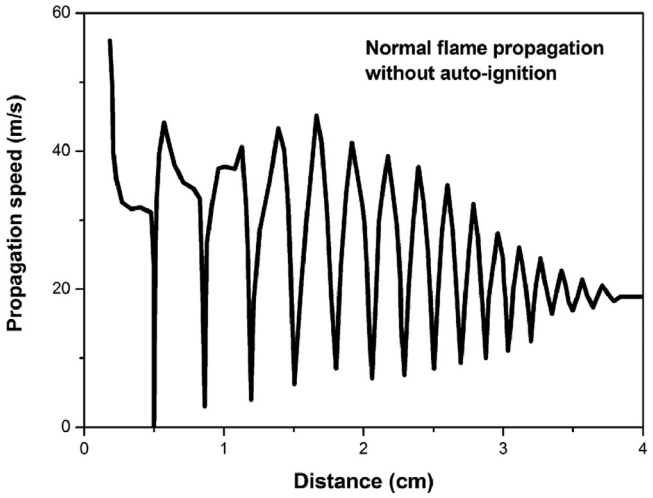

Fig. 3. Transient SI flame speed as a function of spatial position.

speed of 24 m/s, and oscillates due to the pressure waves, as shown in Fig. 3 where the transient SI flame speed at different spatial positions is presented. This pressure wave propagates backward and forward in the closed reactor, which decreases or increases the flame front speed, depending on its propagation direction. The phenomena of pressure fluctuations occur in various closed combustion apparatuses [25–26]. No end-gas auto-ignition occurs throughout this process, as shown by the nearly straight O–A line. However, when T_i is increased to 1000 K, an AI spot occurs at the wall before the arrival of SI flame front, and then an AI reaction front develops to a detonation wave and starts to propagate supersonically towards the SI flame front, with a considerably higher propagation speed of 1624 m/s. Therefore, the entire mixture in the reactor is almost equally consumed by both SI flame and AI reaction front, as shown by the lines of O–B2 and B1–B2. When T_i is further increased to 1050 K, AI spots not only occur at the wall, but also at the region ahead of the SI flame front, such that the entire reactive flows are divided into three parts: normal SI flame front (labeled by O–C1), the first AI reaction front (ARF1, labeled by C1–C3) and the second AI reaction front (ARF2, labeled by C2–C3), with the propagation speed of around 66, 1807 and 1808 m/s, respectively. The initial laminar flame regime first consumes about a quarter of the total mixture in the chamber, and the two AI reaction fronts consume equally on the remained mixture.

These observations basically indicate the significant influence of initial temperature on different reaction fronts in the chamber, involving regular flame front propagation subject to pressure fluctuations, and the fast detonation wave propagation. AI spots can be generated both ahead of the reaction front and in the end-gas at the wall. Investigations on the sequential process of these physical quantities may give insights on the mechanisms of AI spots generation and the transition of deflagration to detonation.

3.2. Pressure mutation and knocking intensity

To illustrate the effect of initial temperature on knocking intensity, the histories of mean thermodynamic states, i.e., pressure and temperature, for the region of x = 3.8–4.0 cm at different initial temperatures are presented in Fig. 4(a) and (b). It shows that the SI flame front propagation acts as an adiabatic compression piston and increases the end-gas pressure and temperature. Once the SI flame front (or new-generated AI reaction front) sweeps the local mixture, its pressure and temperature instantaneously reach the corresponding equilibrium pressure (P_e) and equilibrium temperature (T_e). For the cases of T_i =700 and 800 K, the entire pressure and temperature histories are relatively smooth without obvious oscillations, which can be

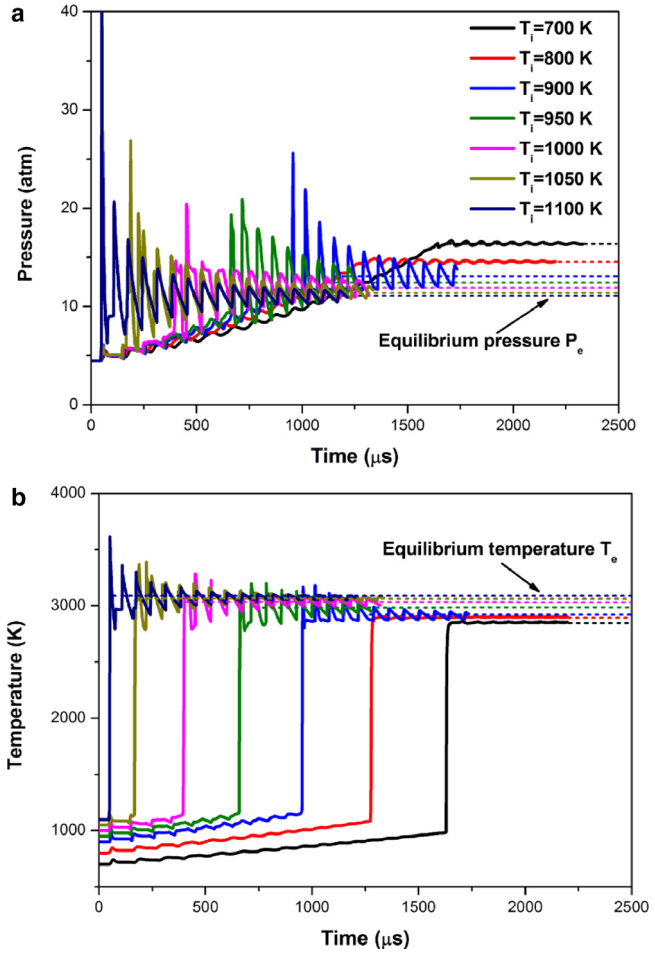

Fig. 4. (a) Mean pressure and (b) mean temperature histories of different initial temperatures for the region of $x = 3.8$–4.0 cm.

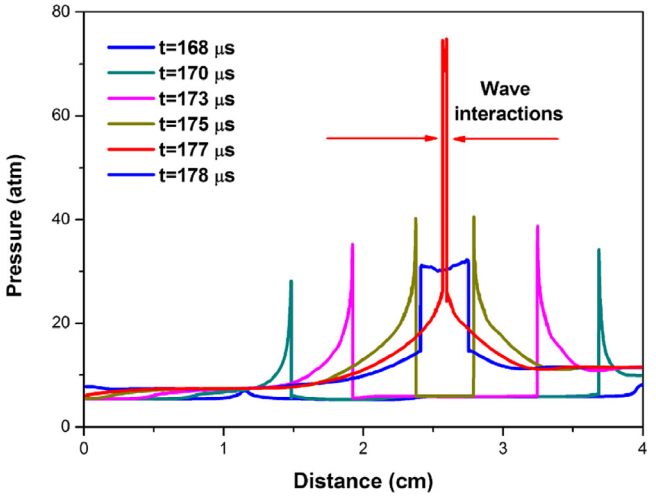

Fig. 5. Temporal sequences of strong pressure wave for initial temperature of T_i = 1050 K.

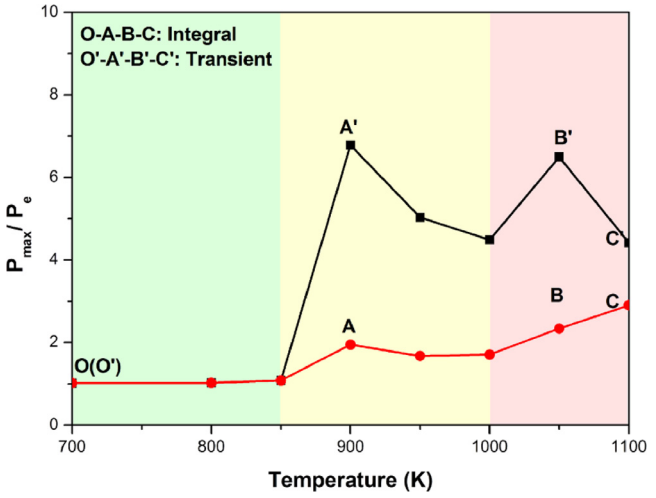

Fig. 6. Knocking intensity as a function of initial temperature from T_i = 700–1100 K.

regarded as knock-free combustion process. With further increases in the initial temperature, auto-ignition will occur locally before the arrival of the SI flame, leading to intensive pressure mutation and strong pressure waves in the end-gas region. Additionally, the onset of pressure oscillation occurs earlier with increasing initial temperature, with non-monotonicity in the magnitude of pressure oscillations, i.e., the magnitude of pressure oscillation of T_i =900 K is even larger than that of T_i =1000 K.

It should be noted that the mean pressure and temperature histories indicate the global knocking intensity for the region of interest [27]. However, to clearly identify the AI spots position and the pressure mutation, accurate temporal resolutions for thermodynamic conditions are necessary. To illustrate this, Fig. 5 shows the evolution of two series of strong pressure waves in the reactor with an initial temperature of T_i =1050 K. It is clearly observed that pressure mutation not only occurs at near-wall region, but also at the region ahead of SI flame front, such that two strong pressure waves propagate reversely, and finally collide with each other at $x \approx 2.6$ cm, leading to a more intense pressure mutation with a magnitude of over 75 atm. Clearly, this physical process has not been captured from the histories of mean pressure and temperature discussed above.

To quantify the pressure mutation characteristics, a knocking intensity $\tilde{P}_{KI}$ is introduced based on the equilibrium pressure P_e and maximum pressure P_{max}:

$$\tilde{P}_{KI} = P_{max}/P_e \tag{5}$$

where P_e is determined from the time history of maximum pressure and P_{max} can be chosen either based on the mean value for the end-gas region of $x = 3.8$–4.0 cm shown in Fig. 4 or during the evolution of whole combustion process throughout the domain shown in Fig. 5.

The results of knocking intensity at different initial temperatures are shown in Fig. 6, where both the integral and the transient results are shown. It is observed that for the integral data labeled by O-A-B-C, the knocking intensity at T_i =900 K exhibits a similar value with that of T_i =1050 and 1100 K, even though the AI occurrence of T_i =900 K case is much later. This observation basically agrees with the previous findings that the knocking severity is not necessarily sensitive to the burned mass fraction (BMF) by end-gas auto-ignition [28]. For the transient form of knocking intensity labeled by O'-A'-B'-C', the variation shows strong non-monotonicity as initial temperature increases beyond 900 K, i.e., the knocking intensity of T_i = 900 K reaches up to $\tilde{P}_{KI} \approx 7$, larger than that of T_i = 950 and 1000 K, corresponding to $\tilde{P}_{KI} \approx 5.3$ and $\tilde{P}_{KI} \approx 4.8$, respectively.

3.3. Interaction of flame fronts and pressure waves

Figure 7 shows the sequential profiles of pressure, temperature and heat release rate as well as their phase contours described by x – t plane for initial temperature of T_i =900 K, where the ARF denotes AI reaction front. It is observed from Fig. 7(a) that before SI flame arrival,

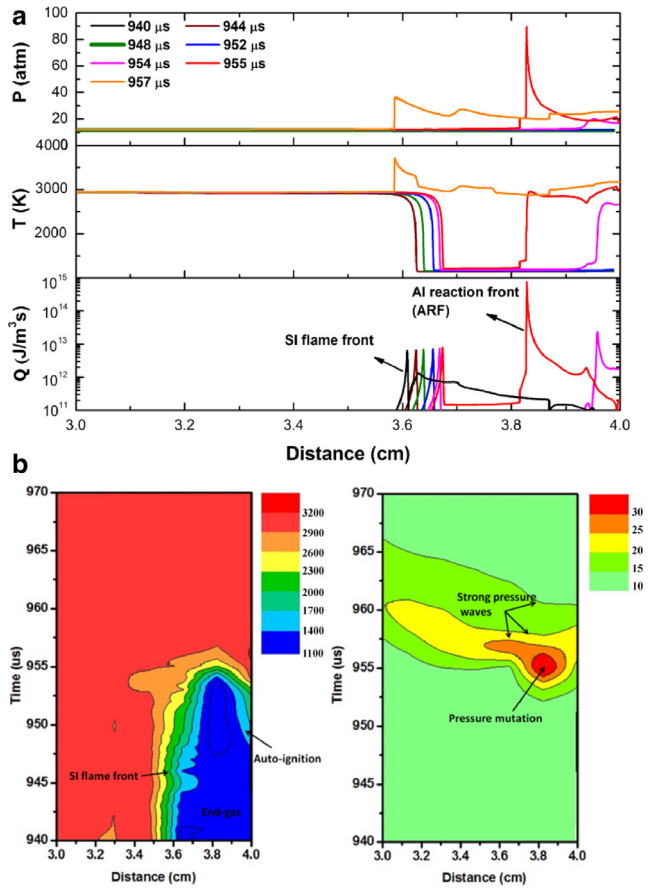

Fig. 7. Sequential profiles of (a) pressure, temperature and heat release rate, and (b) temperature (K) and pressure (atm) contours by $x - t$ plane for $T_i = 900$ K.

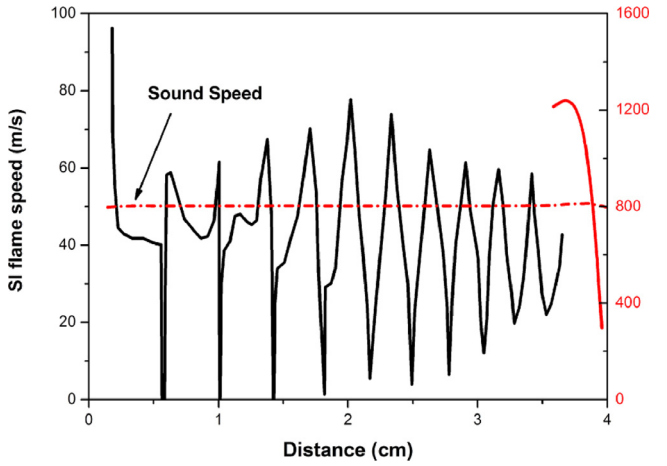

Fig. 8. Transient speed of SI flame front, AI reaction front and sound speed ahead of reaction fronts for $T_i = 900$ K.

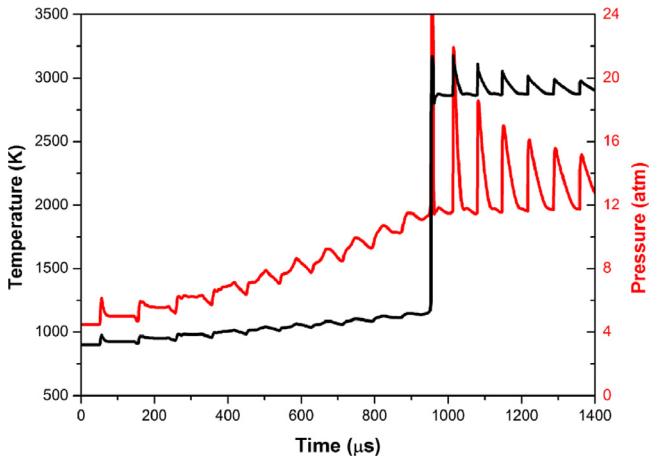

Fig. 9. Temporal evolution of temperature and pressure of the mixture at right wall for $T_i = 900$ K.

an AI spot starts to occur at the near-wall region, followed by a pressure mutation and strong pressure wave propagation. Then the strong pressure wave couples with the AI reaction front to form a detonation wave, propagating towards the SI flame front, with a much higher speed compared to the SI flame. Meanwhile, the heat release rate of the AI reaction front is three orders of magnitude higher than that of the SI flame front, consequently showing a much stronger thermal expansion effect. Due to the stronger compression waves from the end-gas, the SI flame front propagates forward more slowly and even goes backwards. Compared to the SI flame front, the AI reaction front seems to exhibit an accelerating behavior, without being affected by the thermal expansion of the SI flame. Detailed evolution of end-gas auto-ignition and pressure wave development can be further found in Fig. 7(b). It is observed that obvious local temperature gradients are first induced at near-wall region before the end-gas auto-ignition, and the AI reaction front starts to propagate inversely to the SI flame front, while generating pressure waves. Sequentially, the pressure wave becomes increasingly stronger, and eventually an intense pressure mutation is formed at $x \approx 3.8$ cm near the wall region.

Due to the inherently different physics, the velocity scales associated with the flame front propagation, pressure wave and auto-ignition of the local mixture are largely different. Figure 8 shows the transient propagation speed of SI flame front, AI reaction front and local sound speed ahead of reaction front. It is observed that before end-gas auto-ignition, the pressure wave propagate backward and forward with a local sound speed of around 800 m/s. Consequently, the profile of SI flame front propagation exhibits an oscillating behavior as in the case of $T_i = 700$ K, but with a mean deflagration flame speed of 35 m/s. On the contrary, the AI reaction front propagates much faster. Once auto-ignition occurs, the corresponding reaction front could propagate at a speed up to over 1200 m/s, still much lower than a fully developed steady CJ detonation speed of about 1900 m/s for the same mixture under 4.5 atm and 900 K, indicating the lack of sufficient domain for its transition. Temperature and pressure history of the local mixture near the wall is further plotted to show the effect of the fluctuations of the thermodynamic conditions on the occurrence of auto-ignition, as show in Fig. 9. It is observed that before auto-ignition, the local mixture has been disturbed by pressure wave by 9–10 times, and for each time, the local temperature and pressure will be increased by the reflection of the pressure wave from the wall. Due to the inherent sensitivity of chemical reactions to temperature and pressure, these fluctuations make ignition much faster than under constant state conditions, demonstrating the significant effect of pressure wave on the end-gas auto-ignition process. On the other hand, the occurrence of auto-ignition near the wall in turn generates pressure wave with much higher magnitude, which further affects the SI flame propagation.

Figure 10 shows the sequential profiles of pressure, temperature and heat release rate and the phase diagram of pressure and temperature for T_i=1050 K. It is observed from Fig. 10(a) that AI spots simultaneously take place not only at the near-wall region, but also at the position ahead of SI flame front. Violent heat release from these AI spots then generates two series of pressure wave and forms two detonated AI reaction fronts propagating towards each other, with increasing magnitudes of temperature and pressure. These two reversely propagating reaction fronts eventually collide with each other

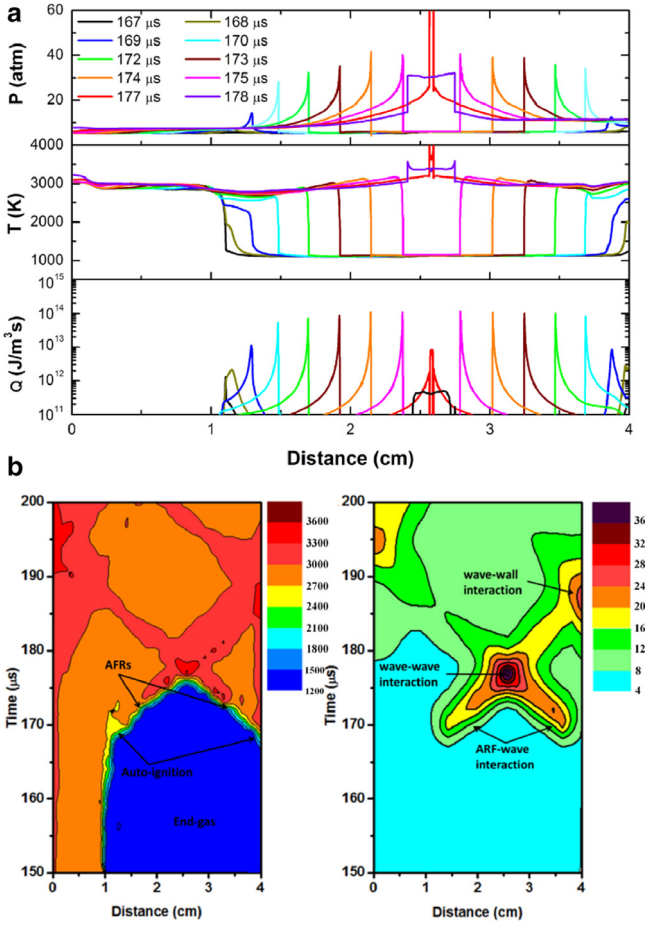

Fig. 10. Sequential profiles of (a) pressure, temperature and heat release rate, and (b) temperature (K) and pressure (atm) contours by $x-t$ plane for $T_i = 1050$ K.

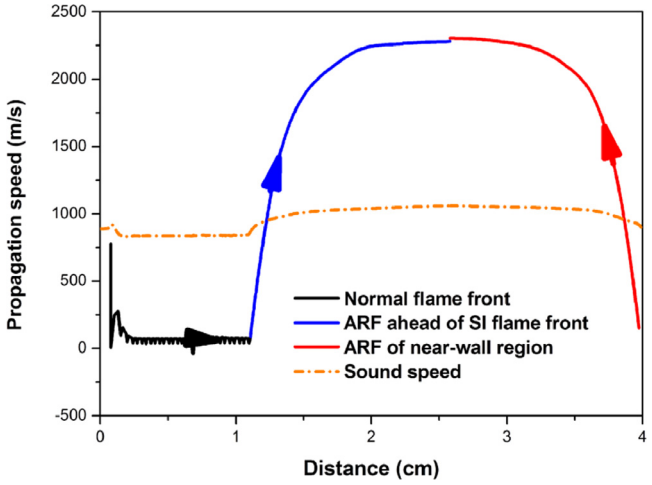

Fig. 11. Transient reaction front speed and sound speed ahead of the different reaction fronts for $T_i = 1050$ K.

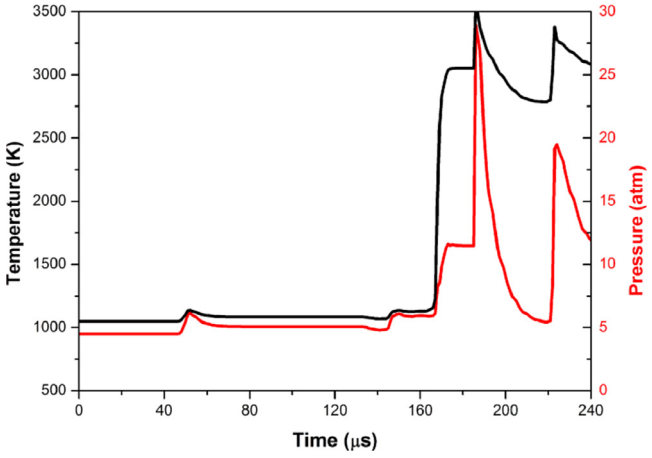

Fig. 12. Temporal evolution of temperature and pressure of the mixture at the wall for $T_i = 1050$ K.

at $x \approx 2.6$ cm, leading to an intense local pressure mutation through wave superposition. It is noted that the duration of the pressure wave is typically the transit time across the detonation, as also shown in [29]. Complete physical process for AI generation and the interactions between reaction front and pressure wave can be found in Fig. 10(b). In this case, the complicated combustion scenario could be further decoupled, namely, wave–wall interaction at the wall, wave–wave interaction by superposition effect and reaction fronts–wave interaction, and these processes interact with each other thermodynamically and/or chemically. It should be noted that the initial pressure mutation directly induced by auto-ignition is not as severe as that in the case of $T_i = 900$ K, but the later developed pressure mutation becomes much more intense as a result of the wave interactions.

To further illustrate the combustion characteristics of both AI reaction fronts for T_i=1050 K, transient reaction front speed and local sound speed just ahead of the reaction front are presented in Fig. 11. It is observed that at the beginning, the SI flame front propagates at a deflagration speed, with a strong oscillation due to the disturbance caused by the pressure wave in the closed reactor. Then two AI reaction fronts are initiated at different locations, and then quickly transit across sonic and develop into supersonic detonation modes from the coupling between pressure wave and reaction front. This detonation speed could be over 2200 m/s, reaches maximum in the high-pressure wave collision zone, even higher compared to the CJ detonation speed of 1950 m/s for stoichiometric H_2/air mixture under 1050 K and 10 atm. This might result from the elevation of local thermodynamic conditions during the wave interactions and the feeding of reactive radicals prepared by auto-ignition to the detonation wave front. Furthermore, temporal evolutions of temperature and pressure of the mixture at the wall are presented in Fig. 12, to illustrate the effect of pressure wave on the end-gas auto-ignition. It is observed that due to the much faster reaction front propagation compared to the T_i=900 K case, the pressure wave has been reflected at the wall by only twice before auto-ignition, followed by much larger pressure and temperature fluctuations thereafter.

When initial temperature is further increased to T_i=1100 K, AI spots only take place at the position ahead of SI flame front and no auto-ignition event occurs at the near-wall region, as shown in Fig. 13. In this case, an AI spot occurring at $x \approx$ 0.25 cm results in a considerable local pressure mutation and subsequent pressure wave propagation. Then an AI reaction front is initiated and quickly accelerates due to the coupling with pressure wave, and eventually develops into a steady supersonic detonation wave with a pressure peak of $P_{max} \approx$35 atm. The entire mixture in the reactor is consumed by the fast propagating reaction front, and finally the strong wave is reflected at the wall, with a pressure increase by a factor of 2. The transient reaction front speed and local sound speed are shown in Fig. 14, which indicates that after the occurrence of auto-ignition ahead of the SI flame front, flame speed transitions from deflagration to detonation mode with a propagation speed of up to 2300 m/s, again higher than the corresponding CJ detonation velocity for stoichiometric H_2/air under similar thermodynamic conditions. This combustion process may also occur in controlled auto-ignition (CAI)

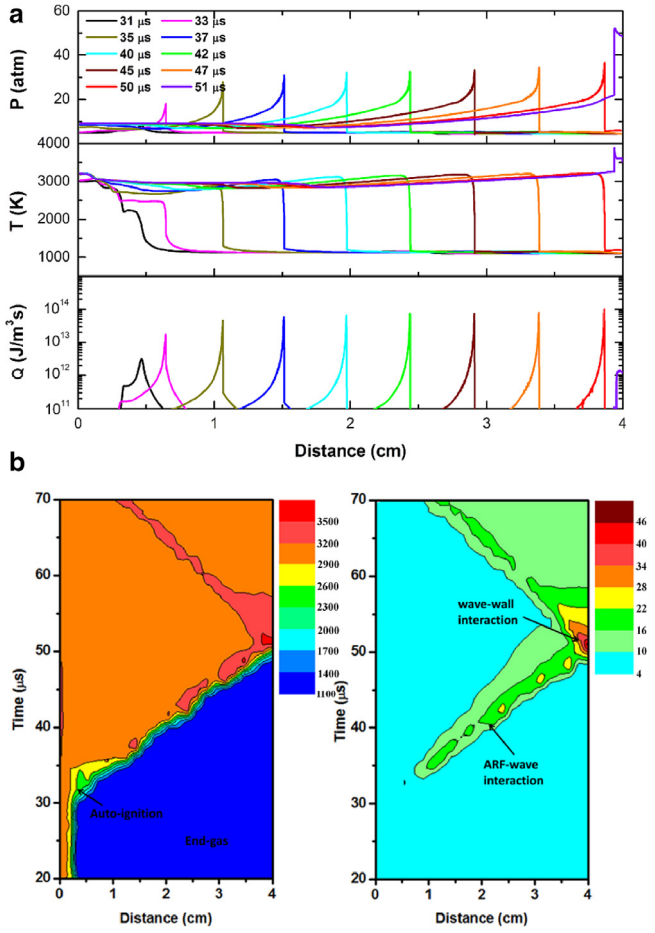

Fig. 13. Sequential profiles of (a) pressure, temperature and heat release rate, and (b) temperature (K) and pressure (atm) contours by $x-t$ plane for $T_i = 1100$ K.

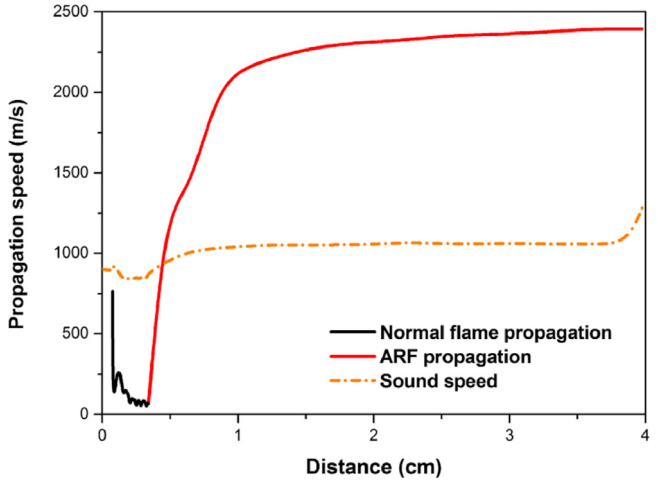

Fig. 14. Transient reaction front speed and sound speed ahead of the reaction fronts for $T_i = 1100$ K.

engines where the mixture is sufficiently reactive to support a developing detonation [30]. Although no auto-ignition occurs in near-wall region for this case, the temporal evolution of temperature and pressure of the mixture at right wall are still shown in Fig. 15. It is observed that unlike previous cases, the local mixture is not disturbed by pressure wave, such that the temporal temperature and pressure of local mixture stays constant before the arrival of AI reactive front. This is due to the fact that the AI reactive front generated at the flame

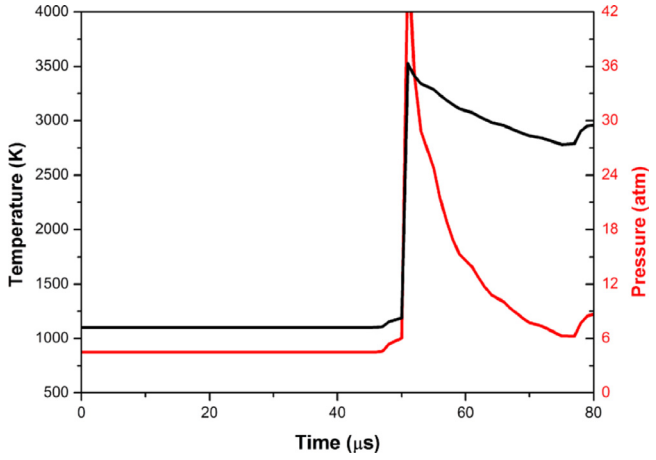

Fig. 15. Temporal evolution of temperature and pressure of the mixture at the wall for $T_i = 1100$ K.

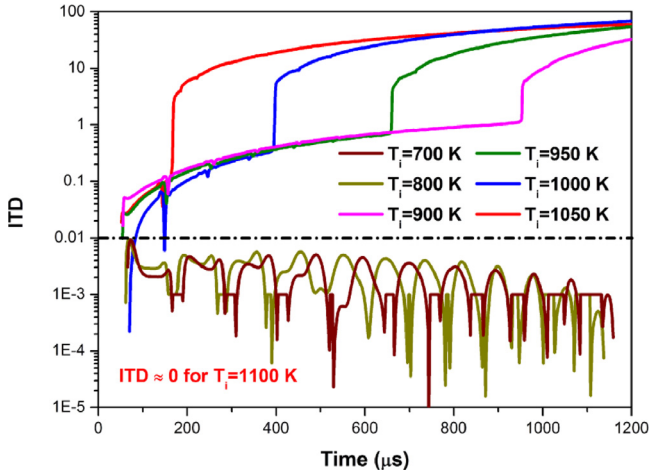

Fig. 16. Evolution of the integrals of dimensionless temperature difference.

front quickly develops into detonations and propagates so fast that the pressure wave is caught up with before reaching the wall region.

With the combustion scenarios at different initial temperatures discussed above, a first major phenomenon is the auto-ignition process of the mixture near the wall. Contrary to the constant-state ignition occurs in shock tubes and rapid compression machines, the thermodynamic condition of the end-gas is strongly affected by the fluctuations caused by the pressure wave, when the initial temperature is not too high (below 1100 K). In other words, it is necessary to evaluate the thermal inhomogeneity of mixture induced by pressure wave propagation at the near-wall region. Here, an integral of dimensionless temperature difference (ITD) has been utilized to quantify the inhomogeneous temperature distributions [17]:

$$ITD = \frac{1}{T_i}\int_0^t (T_{x=4.0} - T_{x=3.8})dt \tag{6}$$

where T_i is the initial temperature at the time of t =0, $T_{x=j}$ the temperature at $x = j$ cm and t is the elapsed time. The ITD represents the accumulation of temperature difference between the two points of interest, and the higher the ITD, the larger the inhomogeneity of spatial temperature distributions.

Figure 16 shows the results of integral evolution of dimensionless temperature difference for initial temperature of T_i =700–1100 K. It is observed that for all cases with pressure wave disturbance, the ITD shows a positive value, indicating that the temperature at the wall (x =4.0 cm) is higher than that at the position of x =3.8 cm, from

an integration perspective. Furthermore, for the cases of T_i =700 and 800 K without auto-ignition, their ITDs do not continually increase with time, instead, they fluctuates below a small value. However, the ITD experiences a continuous accumulation and increases to a large value for the four cases of T_i =900–1050 K, where there is an auto-ignition event induced by pressure wave disturbance in the near-wall region. For the case of T_i =1100 K, the ITD is approximately equal to zero due to the lack of pressure wave arrival. These results basically indicate the ITD is a good metric to evaluate the propensity of auto-ignition events subject to temperature inhomogeneity. It therefore implies that the thermal inhomogeneity induced by pressure wave disturbance plays an important role for the auto-ignition at near-wall region.

3.4. Auto-ignition position transition

From the above discussions, we have clearly demonstrated the behavior of flame propagation and pressure mutation, pressure wave interaction, as well as the mechanism of end-gas auto-ignition event with pressure wave disturbance. However, the underlying reasons for another major phenomenon on the AI spot generation ahead of flame front and the auto-ignition position transition have not been fully revealed. Specifically, we shall provide a detailed explanation on the fact that no auto-ignition occurs at the near-wall region for T_i =1100 K, and that there is an auto-ignition event occurring at the position ahead of flame front for the initial temperature above 1050 K.

Firstly, we have changed the original chamber length into $L = 3.0$ and 6.0 cm for the initial temperature 1100 K case respectively, to demonstrate the residence time effect on the end-gas auto-ignition. For the case of $L = 3.0$ cm, the mixture at the right wall is affected by pressure wave, such that thermal inhomogeneity should exist before the arrival of reaction front; while there should be homogeneous temperature distributions at the near-wall region due to the lack of pressure wave disturbance for the case of $L = 6.0$ cm. Figure 17 shows the results of temporal temperature distributions of the mixture in the closed reactor. It is observed from Fig. 17(a) that unlike the case of $L = 4.0$ cm in Section 3.3, there is a large temperature inhomogeneity in the mixture at the right wall at $t = 44$ μs and an auto-ignition event occurs at the $t = 45$ μs. According to previous analysis, this auto-ignition event should be attributed to the thermal inhomogeneity induced by pressure wave disturbance. For the case of $L = 6.0$ cm, Fig. 17(b) shows that there is no pressure wave disturbance in the local mixture near the wall due to the fast detonation propagation mode, and therefore the auto-ignition occurred in the end-gas is purely a homogeneous thermal explosion. Meanwhile, it is noted that in the case of $L = 6.0$ cm, there is no auto-ignition occurrence when the reaction front arrives at $x = 4.0$ cm. This could be due to the fact that the local mixture is not sufficiently reactive to auto-ignite. Furthermore, the ignition delay time of different thermodynamic states around T_i=1050 K and 1100 K are presented in Fig. 18, which shows that in the temperature range of 1050–1150 K, ignition delay time is very sensitive to temperature, which may be another reason for the auto-ignition transition of the mixture at near-wall region.

Secondly, it is interesting to find that there is a transition for the auto-ignition occurrence from the end-gas to the location ahead of flame front, and the AI spot is able to further develop into a (developing) detonation wave. Basically, such an auto-ignition event results from the interaction of pressure wave and flame structure when the temperature and pressure of the local mixture corresponds to an ignition delay that is not too long and also sufficiently sensitive to the thermodynamic conditions [6].

Figure 19 shows the temporal evolution of temperature and pressure at different positions in the preheat zone of flame front for the case of T_i=1100 K. It is seen that at the beginning, the temperature and pressure are the same for these selected positions; when

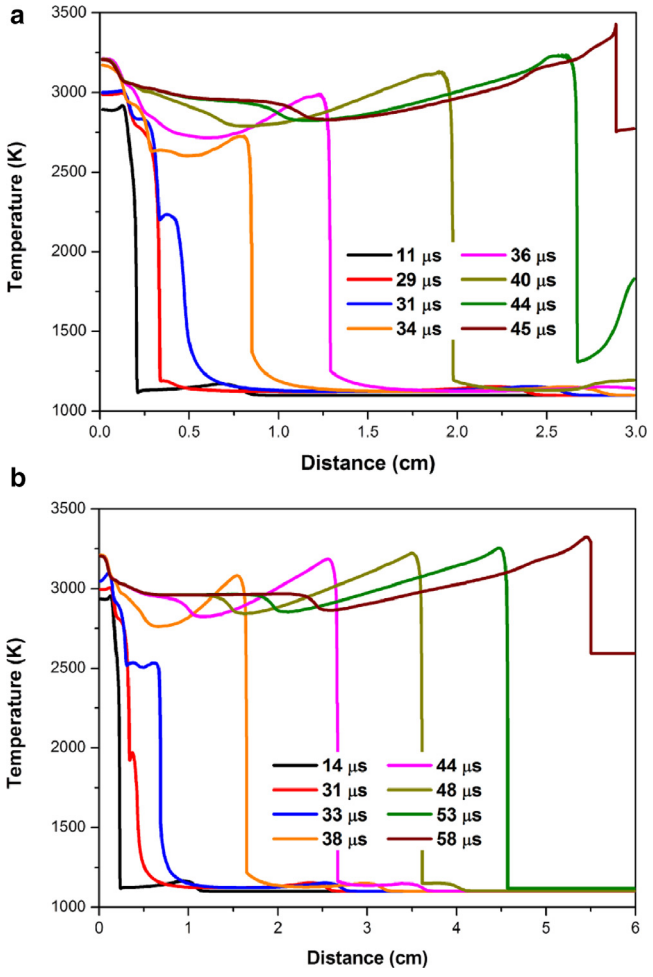

Fig. 17. Temporal temperature distributions of the mixture in the reactor with (a) L = 3.0 cm and (b) $L = 6.0$ cm for $T_i = 1100$ K.

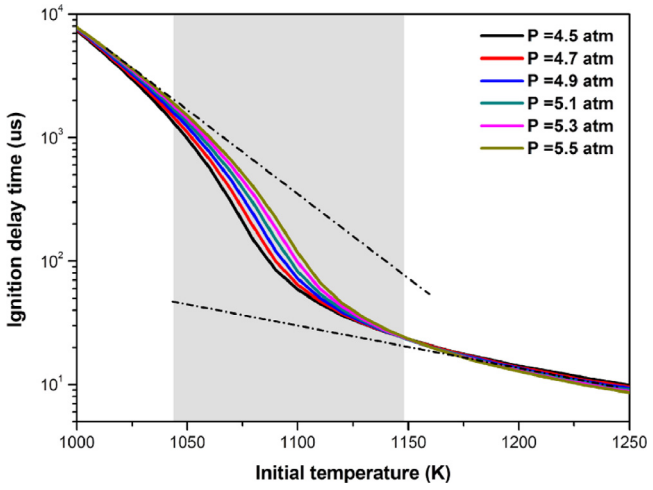

Fig. 18. Ignition delay time as a function of initial temperature and pressure of homogeneous stoichiometric H_2–air mixture.

$t \leq 28.5$ μs, the pressure is nearly uniformly distributed, but it shows an obvious temperature gradient in the preheat zone of the flame front. Moreover, the closer the selected position to the flame front, the earlier the temperature gradient appears. This observation suggests the direct thermal effect of flame front on the AI spot generation. In addition, Fig. 20 shows corresponding temperature and pressure distributions during AI spot generation near the flame front.

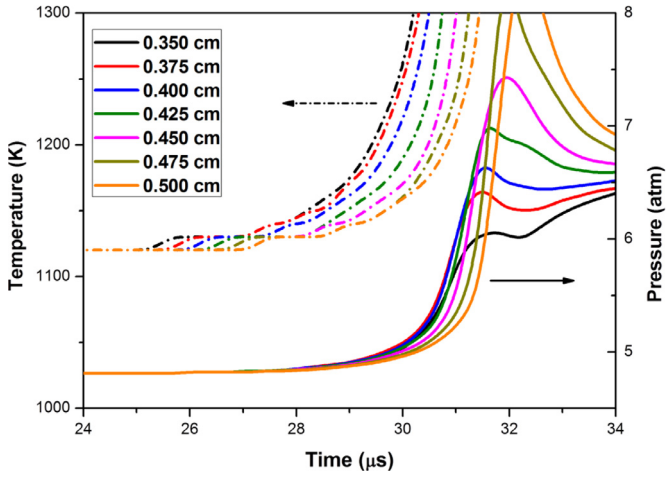

Fig. 19. Temporal evolution of temperature and pressure at different position in the preheat zone of flame front for $T_i = 1100$ K.

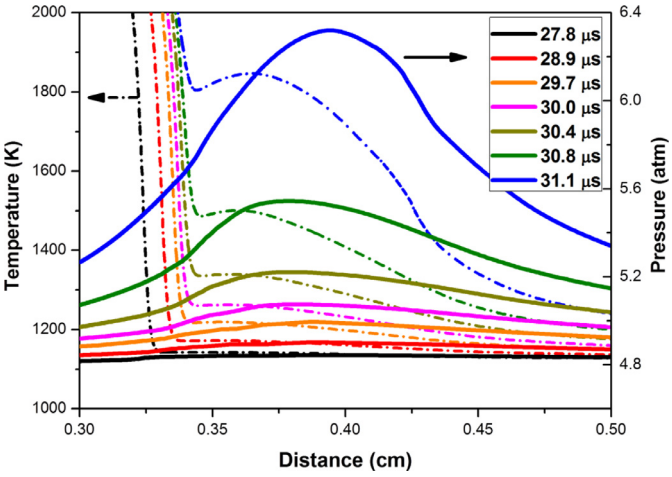

Fig. 20. Evolution of temperature (dash) and pressure (line) distributions during auto-ignition development ahead of flame front for $T_i = 1100$ K.

It can be observed that due to the heat release of local auto-ignition in preheat zone of flame front, a local pressure mutation is generated, followed by a pressure wave propagating forward. Because the pre-mixture is on the threshold of auto-ignition, the propagation of pressure wave will increase the temperature and pressure of adjacent mixture and thus decrease ignition delay of the local mixture. Therefore, new auto-ignition spots will be induced and then couple with the flame front during its propagation. Initially, the pressure wave propagates at the head of reaction front, as shown in Fig. 20. Then the reaction front accelerates to catch up with the pressure wave and couples with it, eventually leading to the generation of stronger pressure wave and detonations, as shown in Fig. 13.

To further explain the occurrence of the auto-ignition at the foot of the preheated zone, it should be noted that although the temperature within the flame is higher, due to the large slope of temperature and concentration, reactive radicals diffuse really fast out of a potential kernel, which could further be consumed by the propagation of the flame without causing local pressure/temperature build-up because of the limited residence time. On the contrary, for a potential auto-ignition spot in the upstream, there is much longer residence time for the particle to ignite. In addition, the flame back diffusion can feed reactive radicals into the ignition kernel, being more intense when the flame propagates closer. Therefore, both the longer residence time and the stronger back diffusion due to the approaching flame allows local temperature/pressure to build up and facilitate the auto-ignition process in the preheat zone.

Conclusions

One dimensional direct numerical simulation with detailed kinetics and transport property was performed in a closed constant volume reactor to investigate the detailed interaction mechanisms of flame front propagation, auto-ignition and pressure wave during knocking combustion, with special emphasis on auto-ignition occurrence and pressure mutation generation in the reactive flows.

First, the binary interactions of SI flame propagation, AI spots generation and pressure wave are significantly influenced by initial temperatures. As initial temperature increases, there is a transition for the AI position from the near-wall region to the region ahead of SI flame front. For the auto-ignition occurring ahead of flame front, it is demonstrated that that the dominant mechanism is the interaction of pressure wave and flame structure, where the local auto-ignition in flame preheat zone facilitates the detonation development. The pressure fluctuation during the auto-ignition ahead of flame further couples with the flame front to facilitate its transition to developing detonation waves.

Second, it is shown that knocking intensity is not only related to initial auto-ignition events, but also to the intense pressure mutation induced by the interactions of flame front propagation, AI reaction front and pressure waves, involving wave-wave interaction, wave-wall interaction and reaction front-wave interaction, etc. The collision of the two AI reactions front under certain condition could cause extremely intense pressure mutations in the chamber. Furthermore, the integral of dimensionless temperature difference analysis shows that the thermal inhomogeneity of the mixture induced by pressure wave disturbance plays an essential role in auto-ignition occurrence at the near-wall region.

Third, detailed analysis has been further performed based on the propagation velocities of various sub-processes, including the flame front propagation, detonating AI reaction front and the pressure waves, as well as tracing the thermodynamic conditions at different AI spots both at end mixture and ahead of flame front. The entire combustion process depends on the velocity (time) scales of flame propagation, pressure wave and ignition delay of local mixture. Simulations with different chamber lengths shows different end-gas auto-ignition mechanism: with longer residence time, pressure wave is caught up with the detonation front, leading to constant-state homogeneous auto-ignition; while with shorter residence time, the pressure wave causes local temperature homogeneity to promote auto-ignition.

It is noted that the present study aims to analyze the fundamental interactions of major physical elements involved in knock and super-knock combustion, which facilitates future studies with further guidance towards the practical situations, with realistic fuel properties, thermodynamic conditions, and flow characteristics.

Acknowledgment

This work was supported by the National Natural Science Foundation of China (Grant no. 51476114, 51176138).

Reference

[1] P. Leduc, B. Dubar, A. Ranini, G. Monnier, Downsizing of Gasoline engine: an efficient way to reduce CO_2 emissions, Oil Gas Sci. Technol. - Rev. IFP 58 (2003) 115–127.
[2] C. Stovell, J. Chiu, R. Hise, P. Swenson, Effect of reduced boost air temperature on knock limited brake mean effective pressure (BMEP), SAE Technical Paper, 2001-01-3682, 2001.
[3] J.Y. Pan, G.Q Shu, H.Q. Wei, Research on in-cylinder pressure oscillation characteristic during knocking combustion in spark-ignition engine, Fuel 120 (2014) 150–157.
[4] Y. Yang, J.E. Dec, N. Dronniou, M. Sjöberg, Partial Fuel Stratification to control HCCI heat release rates: fuel composition and other factors affecting pre-ignition reactions of two-stage ignition fuels, SAE Technical Paper, 2011-01-1359, 2011.

[5] J.Y. Pan, G.Q. Shu, H.Q. Wei, Interaction of flame propagation and pressure waves during knocking combustion in spark-ignition engines, Combust. Sci. Technol. 186 (2014) 192–209.
[6] Y.B. Zeldovich, Regime classification of an exothermic reaction with nonuniform initial conditions, Combust. Flame 39 (1980) 211–214.
[7] D. Bradley, Autoignitions and detonations in engines and ducts, Philos, Trans. A Math. Phys. Eng. Sci. 370 (2012) 689–714.
[8] X. Gu, D. Emerson, D. Bradley, Modes of reaction front propagation from hot spots, Combust. Flame 133 (2003) 63–74.
[9] G. Kalghatgi, Developments in internal combustion engines and implications for combustion science and future transport fuels, Proc. Combust. Inst. 35 (2015) 101–115.
[10] J.F. Griffiths, J.P. MacNamara, C.G.W. Sheppard, D.A. Turton, B.J. Whitaker, The relationship of knock during controlled autoignition to temperature inhomogeneities and fuel reactivity, Fuel 81 (2002) 2219–2225.
[11] P. Dai, Z. Chen, S. Chen, Y. Ju, Modes of reaction front propagation in n-heptane/air mixture with temperature gradient, Proc. Combust. Inst. 35 (2015) 3045–3052.
[12] W.J. Pitz, C.K. Westbrook, Dynamics of reactive systems part ii: modeling and heterogeneous combustion, in: J.R. Bowen, J.C. Leyer, R.I. Soloukhin (Eds.), Progress in Astronautics and Aeronautics Series, American Institute of Aeronautics and Astronautics, New York, 1986, pp. 293–303.
[13] J.B. Martz, H. Kwak, H.G. Im, G.A. Lavoie, D.N. Assanis, Combustion regime of a reacting front propagating into an auto-igniting mixture, Proc. Combust. Inst. 33 (2011) 3001–3006.
[14] J.B. Martz, G.A. Lavoie, H.G. Im, R.J. Middleton, A. Babajimopoulos, D.N. Assanis, The propagation of a laminar reaction front during end-gas auto-ignition, Combust. Flame 159 (2012) 2077–2086.
[15] Y. Ju, W. Sun, M.P. Burke, X. Gou, Z. Chen, Multi-timescale modeling of ignition and flame regimes of n-heptane-air mixtures near spark assisted homogeneous charge compression ignition conditions, Proc. Combust. Inst. 33 (2011) 1245–1251.
[16] A. Robert, S. Richard, O. Colin, T. Poinsot, LES study of deflagration to detonation mechanisms in a downsized spark ignition engine, Combust. Flame 162 (2015) 2788–2807.
[17] H. Terashima, M. Koshi, Mechanisms of strong pressure wave generation in end-gas autoignition during knocking combustion, Combust. Flame 162 (2015) 1944–1956.
[18] E.S. Oran, V.N. Gamezo, Origins of the deflagration-to-detonation transition in gas-phase combustion, Combust. Flame 148 (2007) 4–47.
[19] Z. Chen, M.P. Burke, Y. Ju, Effects of Lewis number and ignition energy on the determination of laminar flame speed using propagating spherical flames, Proc. Combust. Inst. 32 (2009) 1253–1260.
[20] R. Kee, J. Grcar, M. Smooke, J. Miller, A fortran program for modeling a steady laminar one-dimensional premixed flame, Sandia Report No. SAND85-8240, Sandia National Laboratories, Livermore, CA, USA, 1987.
[21] Z. Chen, On the extraction of laminar flame speed and Markstein length from outwardly propagating spherical flames, Combust. Flame 158 (2011) 291–300.
[22] W.K. Zhang, Z. Chen, W.J. Kong, Effects of diluents on the ignition of premixed H_2/air mixtures, Combust. Flame 159 (2012) 151–160.
[23] Z. Chen, Studies on the initiation, propagation, and extinction of premixed flames, Ph.D. Thesis, Princeton University, Princeton, NJ, USA, 2008.
[24] M.P. Burke1, M. Chaos, Y. Ju, F.L. Dryer1, S.J. Klippenstein, Comprehensive H_2/O_2 kinetic model for high-pressure combustion, Int. J. Chem. Kinet. 44 (2012) 444–474.
[25] C. Jiménez, J. Quinard, J.G. Otero, H. Schmidt, G. Searby, Unsteady response of hydrogen and methane flames to pressure waves, Combust. Flame 159 (2012) 1894–1908.
[26] H. Xiao, X. Shen, J. Sun, Experimental study and three-dimensional simulation of premixed hydrogen/air flame propagation in a closed duct, Int. J. Hydrogen Energy 37 (2012) 11466–11473.
[27] J. Pan, C. Sheppard, A. Tindall, M. Berzins, S.V. Pennington, J.M. Ware, End gas inhomogeneity, autoignition and knock, SAE Technical Paper, 1998–98–2616, 1998.
[28] G. Konig, C. Sheppard, End gas autoignition and knock in a spark ignition engine, SAE Technical Paper, 1990 –90–2135, 1990.
[29] R. Courant, K.O. Friedrichs, Supersonic flow and shock waves, New York University, New York, 1948.
[30] D. Bradley, C. Morley, X. Gu, D. Emerson, Amplified pressure waves during autoignition: relevance to CAI engines, SAE Technical Paper, 2002-01-2868, 2002.